Int. J. Heat Mass Transfer. Vol. 36, No. 9, pp. 2305–2315, 1993
Printed in Great Britain

0017-9310/93 $6.00 + 0.00

Finite-amplitude instability of mixed-convection in a heated vertical pipe

B. B. ROGERS and L. S. YAO
Department of Mechanical and Aerospace Engineering, Arizona State University, Tempe, AZ 85287, U.S.A.

(*Received* 1 *July* 1992 *and in final form* 27 *October* 1992)

Abstract—The instability of flow in a heated vertical pipe is studied using weakly nonlinear instability theory for both stably and unstably stratified cases. It is found that the dominant instability for stably stratified flow is a thermal-buoyant instability, while that of the unstably stratified case is a Rayleigh–Taylor instability. The weakly nonlinear theory predicts supercritical instability for the stably stratified case, in agreement with experimental observations. In this case, it is found that a wide band of wave numbers are linearly unstable soon after the onset of the initial instability. This limits the range for which the weakly nonlinear results are accurate in this case since the theory considers the growth of a single dominant wave. The results of the weakly nonlinear calculations for unstably stratified flow indicate that the flow is potentially subcritically unstable, again in agreement with the experimental observations. On the other hand, the theory predicts that a large amplitude disturbance will be necessary to initiate subcritical instability, while the amplitude of a supercritical disturbance will grow quickly as the magnitude of Ra increases. Therefore, another possible flow transition that is consistent with experimental observations involves rapid growth of the first azimuthal mode of a supercritical Rayleigh–Taylor instability, followed by secondary instabilities that lead quickly to turbulence. Analysis of energy transfer in the fundamental wave demonstrates that the thermal-buoyant instability is supercritical because increases in the viscous dissipation rate and the rate of transfer of energy from the fundamental wave back into the mean flow overcome the destabilizing effect of an increase in the rate of buoyant production. Subcritical instability occurs with the Rayleigh–Taylor mode when the disturbance amplitude increases to the point that the combined destabilizing effects caused by a change in the shape of the fundamental wave induced by nonlinear effects become larger than the stabilizing effects due to the production of the harmonic wave and the distortion of the mean-flow. The increase in heat transfer rates due to instability predicted by the weakly nonlinear theory is smaller than the experimental observations. However, it is demonstrated that experimentally observed increases in Nu are predicted if the effects of additional waves are included in an approximate manner.

1. INTRODUCTION

MIXED convection in a vertical circular pipe is a fundamental convection problem. Unfortunately, our understanding of this motion and the associated heat transfer mechanisms is incomplete. An example of this lack of understanding is often found in the analysis of fully-developed mixed-convection in ducts, where it is common practice to treat the problem as a parallel flow, ignoring the possibility of thermally induced hydrodynamic instabilities. The parallel flow assumption greatly simplifies the analysis since the velocity and temperature fields then become easily predicted functions of the transverse variables only. However, as was demonstrated in refs. [1, 2], fully developed mixed-convection in a vertical pipe is highly unstable due to thermal effects, and a parallel flow will be observed in the laboratory only under special conditions. Therefore, the parallel flow assumption is inadequate to describe mixed-convection in vertical ducts, since the presence of flow instabilities will give rise to an unsteady, three-dimensional motion. The proper analysis of these problems must consider the nonlinear growth of secondary flow patterns induced by instability. Therefore, in this paper, we will study these effects by using the weakly nonlinear instability theory to model the finite-amplitude behavior of unstable disturbances in mixed-convection in a vertical pipe.

Experimental observations of mixed-convection in heated vertical pipes indicate that the flow becomes unstable due to thermal effects at low heating rates, and at Reynolds numbers as low as 30 [3–5]. The effects of the disturbances on heat transfer rates were substantial, with increases of 30% observed after the onset of instability. When the flow is stably stratified so that the density is decreasing in the upward direction, such as upward flow in a heated pipe, the initial transition resulted in a new equilibrium, nonparallel flow that was highly structured. On the other hand, when the flow was unstably stratified, such as in upward flow in a cooled pipe, the observed transition to turbulence was more abrupt, although a tendency for the flow to become asymmetric soon before transition was observed. Therefore, in the stably stratified case, the instability is supercritical. However, in the unstably stratified case, the initial instability may itself be subcritical, or the transition may be due to a secondary instability caused by the growth of an asymmetric supercritical disturbance.

The linear-instability analysis of Yao [1, 2] demonstrated that heated flow in a vertical pipe is unstable

NOMENCLATURE

A	order $(c_i)^{1/2}$ amplitude
a_1	first Landau constant, $a_{1r}+ia_{1i}$
B	order one amplitude
E_s	fraction of shear energy production at the neutral curve
E_b	fraction of buoyant energy production at the neutral curve
E_d	viscous dissipation of kinetic energy at the neutral curve
$\mathbf{E}_{12}$	energy transferred to harmonic wave due to nonlinear effects
c	complex disturbance wave speed, c_r+ic_i
D^2	operator in equation (1)
$\mathbf{D}_{11}$	modification of viscous kinetic energy dissipation due to nonlinear effects
g	gravitational acceleration
h	convective heat transfer coefficient
K	curvature parameter for the annulus, $r_i/(r_o-r_i)$
k	fluid thermal conductivity
$\mathbf{L}_0$	linear amplification rate
Nu	Nusselt number, hr_0/k
n	azimuthal wave number
P	pressure
$\mathbf{P}_{101}$	shear energy production by fundamental wave and distorted mean flow
$\mathbf{P}_{110}$	shear energy production by distorted fundamental wave and basic-state
Pr	Prandtl number, ν/γ
r	radial coordinate
r_o	pipe radius
Ra	Rayleigh number, $\mu\beta g(r_o-r_i)^4/\gamma\nu$
Re	Reynolds number, $W_{ave}(r_o-r_i)/\nu$
$\mathbf{T}_{11}$	buoyant energy production by distorted fundamental wave
T_w	pipe wall temperature
t	time
u	radial velocity
v	azimuthal velocity
w	axial velocity
z	axial coordinate.

Greek symbols

α	axial wave number
β	thermal expansion coefficient
γ	thermal diffusivity
η	radial coordinate
θ	dimensionless temperature
μ	vertical temperature gradient
ν	kinematic viscosity
ρ	density
τ	slow time scale, $\tau = t/c_i$
ϕ	azimuthal coordinate.

in most regions of an appropriate parameter space, both for stably and unstably stratified flow. The results for the stably stratified case showed that the flow becomes unstable at $Ra > 70$, and that the critical value of Ra is almost independent of Re for all $Re > 50$. The first azimuthal mode is found to be the least stable mode for all Re except in a narrow band between $Re = 50$ and 150, where the least stable disturbances are axisymmetric. Therefore, the unsteady flow patterns predicted by the linear theory will be a double-spiral flow, in agreement with the experimental observations of Scheele and Hanratty [5]. The results for the unstably stratified case show that the flow will become unstable to the first azimuthal mode at $Ra < -90$, and that the critical value of Ra is again almost independent of Re.

Additional linear-instability studies of mixed-convection in vertical concentric annuli relevant to the present study have been carried out for two types of thermal boundary conditions. In case I, each cylinder was maintained at a different temperature. In case II, a vertical temperature gradient was imposed on the inner cyclinder and the outer cylinder was insulated. For case I, the results for air ($Pr = 0.71$) demonstrated that the instability boundary consists of three distinct instabilities, identified by their characteristic wave numbers and wave speeds [6, 7]. The *shear* instability occurs at large Reynolds numbers. A low Re thermal instability originates with an unstable velocity distribution caused by buoyant forces, but most of the kinetic energy for this instability is obtained by shear production. Therefore, this is a shear instability induced by thermal effects, and is called the *thermal-shear* instability. In this problem, another thermally induced instability appears that bridges the gap between the thermal-shear and the shear instabilities, which also obtains energy primarily through shear production, called the *interactive* instability. Another study, which used the thermal boundary conditions of case II, demonstrated that, in addition to the shear and thermal-shear instabilities, two more thermally induced instabilities may appear [8]. When the vertical temperature gradient is negative, a *Rayleigh–Taylor* type instability is possible since the vertical density stratification is unstable. However, in the stably stratified case, the Rayleigh–Taylor mode is not present, and a thermal instability occurs as the Rayleigh number, which characterizes the magnitude of the vertical temperature gradient in this case, increases. This instability will be a thermal-shear type at small Prandtl numbers, but at large Prandtl numbers another instability appears which obtains kinetic energy primarily by buoyant production, called the *thermal-buoyant* instability.

The results of the linear-instability studies demonstrate that empirical correlations for heat transfer and friction coefficients obtained by using flow transition criteria based on isothermal flows are likely to be incorrect in mixed-convection. On the other hand, linear theory predicts only the onset of instability to infinitesimal disturbances. Therefore, a nonlinear analysis is necessary to study the structure of the flow field that results from linear instability. In this paper, we address this issue by applying the weakly nonlinear theory developed in ref. [9] to the problem of flow in a heated vertical pipe. In Section 2 of the paper the problem is formulated, and the linear and weakly nonlinear instability analyses are developed and explained. The results of the linear-instability analyses of refs. [1, 2] are reviewed in Section 3.1. Analysis of the energy transfer at the neutral curves demonstrates that the least stable modes are the thermal-buoyant mode in the stably stratified case and the Rayleigh–Taylor mode in the unstably stratified case. In Section 3.2, the weakly nonlinear analysis of the stably stratified flow predicts supercritical instability for all wave numbers, in agreement with the experimental observations. The results for the unstably stratified case indicate that the flow is potentially subcritically unstable, again in agreement with the experimental observations. On the other hand, the theory predicts that a large amplitude disturbance will be necessary to initiate subcritical instability, while the amplitude of a supercritical disturbance will grow quickly as the magnitude of Ra increases. Therefore, a possible flow transition will first involve the rapid growth of a supercritical Rayleigh–Taylor instability with an azimuthal wave number of $n = 1$, followed by secondary instabilities that lead quickly to turbulence. As mentioned earlier, this is consistent with the experimental observation of Scheele and Hanratty [5] that the velocity profiles tend to become asymmetric before the unsteady motion sets in.

In Section 3.3, it is demonstrated that the real portion of the first Landau constant, the sign of which predicts whether the instability is subcritical or supercritical, consists of five parts which arise from the following physical processes:

(1) the distortion of the mean motion;
(2) the generation of the harmonic wave;
(3) the modification of the gradient production of disturbance energy due to the change in the shape of the fundamental wave;
(4) the modification of the buoyant production of disturbance energy due to the change in the shape of the fundamental wave;
(5) the modification of the viscous dissipation of the disturbance due to the change in shape of the fundamental wave.

Analysis of these terms for the supercritical thermal-buoyant instability demonstrates that, even though the finite-amplitude effects increase the rate of buoyant production, the net rate of disturbance energy production is decreased by nonlinear effects, leading to a supercritical equilibrium state. This is primarily due to increases in the viscous dissipation rate and the rate of transfer of energy from the fundamental wave back into the mean flow. On the other hand, with the subcritical Rayleigh–Taylor mode, it is found that subcritical instability occurs when the combined destabilizing effects caused by the change in the shape of the fundamental wave, processes 3 through 5 listed above, become larger than the stabilizing effects due to the production of the harmonic wave and the distortion of the mean-flow.

The results in Section 3.1 also demonstrate that a wide band of axial wave numbers become linearly unstable soon after the initial instability. For example, the initial instability occurs at $Ra = 70$, but by $Ra = 75$, all axial wave numbers between 0.04 and 2.7 are linearly unstable. Consequently, even though the weakly nonlinear theory will still be valid in the limit as Ra approaches the critical Rayleigh number, Ra_c, the theory will be inaccurate as Ra increases, since the theory considers only a single dominant unstable wave. This restricts the range for which the weakly nonlinear results will be accurate in this problem. In Section 3.4, the effect of the disturbance growth on heat transfer rates for supercritical instability is analyzed. The results of the weakly nonlinear theory underpredict the experimentally observed increases in Nu due to flow instability. This is because the theory only considers the growth of a single dominant wave. However, it is also demonstrated that the experimentally observed increases in Nu are predicted if the effects of additional waves are included in an approximate manner. On the other hand, a complete description of the problem in this region requires consideration of a continuous band of linearly unstable waves.

2. ANALYSIS

2.1. *Formulation*

The problem being studied is viscous fluid flow driven by an external pressure gradient in a vertical pipe. A constant heat flux is maintained on the outer wall. The governing equations are the Boussinesq equations in cylindrical coordinates:

$$\frac{\partial u}{\partial r} + \frac{u}{r} + \frac{1}{r}\frac{\partial v}{\partial \phi} + \frac{\partial w}{\partial z} = 0 \tag{1a}$$

$$\frac{\partial u}{\partial t} + u\frac{\partial u}{\partial r} + \frac{v}{r}\frac{\partial u}{\partial \phi} + w\frac{\partial u}{\partial z} - \frac{v^2}{r} = -\frac{\partial p}{\partial r} + \frac{1}{Re}\left[\mathrm{D}^2 u - \frac{1}{r^2}\left(2\frac{\partial v}{\partial \phi} + u\right)\right] \tag{1b}$$

$$\frac{\partial v}{\partial t} + u\frac{\partial v}{\partial r} + \frac{v}{r}\frac{\partial v}{\partial \phi} + w\frac{\partial v}{\partial z} + \frac{uv}{r} = -\frac{1}{r}\frac{\partial p}{\partial \phi} + \frac{1}{Re}\left[\mathrm{D}^2 v - \frac{1}{r^2}\left(2\frac{\partial u}{\partial \phi} - v\right)\right] \tag{1c}$$

$$\frac{\partial w}{\partial t}+u\frac{\partial w}{\partial r}+\frac{v}{r}\frac{\partial w}{\partial \phi}+w\frac{\partial w}{\partial z}=-\frac{\partial p}{\partial z}+\frac{1}{Re}[D^2 w]-\frac{Ra}{Re}\theta \tag{1d}$$

$$\frac{\partial \theta}{\partial t}+u\frac{\partial \theta}{\partial r}+\frac{v}{r}\frac{\partial \theta}{\partial \phi}+w\frac{\partial \theta}{\partial z}=\frac{1}{Re\,Pr}[D^2\theta]+\frac{w}{Re\,Pr} \tag{1e}$$

where

$$D^2=\frac{\partial^2}{\partial r^2}+\frac{1}{r}\frac{\partial}{\partial r}+\frac{1}{r^2}\frac{\partial^2}{\partial \phi^2}+\frac{\partial^2}{\partial z^2}.$$

All lengths have been scaled by the radius of the cylinder, r_0, the velocities by the average axial velocity, W_{ave}, the pressure by ρW_{ave}^2 and time by r_0/W_{ave}. The pipe wall temperature, T_w, increases linearly with the axial coordinate as $T_w = T_0+\mu r_0 z$, where T_0 is an upstream reference temperature and z is the dimensionless axial coordinate. A dimensionless temperature has been defined as

$$\theta=\frac{T_w-T}{\mu r_0 Re\,Pr}.$$

Since the temperature is scaled by the vertical temperature gradient μ, the dimensionless temperature will be independent of the axial coordinate, leading to a basic-state which is a function of the radial coordinate only. The parameters in the problem are the Reynolds number, $Re = W_{ave}r_0/\nu$, the Rayleigh number, $Ra = \mu\beta g r_0^4/\gamma\nu$ and the Prandtl number, $Pr = \nu/\gamma$, where ν is the kinematic viscosity, γ the thermal diffusivity, β the thermal expansion coefficient and g the acceleration due to gravity. A positive value of Ra indicates that the fluid temperature is increasing with increasing z. Therefore, the fluid is stably stratified for positive Ra, and unstably stratified for negative Ra.

It is worthwhile to point out that although the problem studied in this paper is that of nonisothermal flow up a vertical pipe, the results may also be used to describe nonisothermal flow down a pipe. This is because the equations governing heated upward flow are identical to those of cooled downward flow, and the equations of cooled upward flow are identical to those of heated downward flow.

2.2. *Basic-state*

The basic-state of the fluid is steady, parallel, laminar fully developed flow. If these assumptions are applied to (1), the basic-state will be a function of the radial coordinate only, and the governing equations will simplify to

$$\frac{d^2W_0}{dr^2}+\frac{1}{r}\frac{dW_0}{dr}-Ra\,\Theta_0=Re\frac{dP_0}{dz} \tag{2a}$$

$$\frac{d^2\Theta_0}{dr^2}+\frac{1}{r}\frac{d\Theta_0}{dr}=-W_0 \tag{2b}$$

where W_0 and Θ_0 represent the basic-state velocity and temperatures respectively. The boundary conditions for the basic-state are

$$\frac{dW_0(0)}{dr}=W_0(1)=\frac{d\Theta_0(0)}{dr}=\Theta_0(1)=0.$$

The effect of the vertical temperature gradient appears in the basic-state energy equation as a non-uniform source term, with a radial distribution and magnitude equal to the basic-state velocity, W_0. Consequently, the basic-state temperature distribution in the radial direction is modified from that which would occur with a uniform wall temperature boundary condition, where there is no vertical temperature stratification. If it is assumed that the axial pressure gradient is constant, the term $Re\,(dP_0/dz)$ may be determined by the requirement of global mass conservation

$$\int_0^1 Wr\,dr=\tfrac{1}{2}$$

and the basic-state becomes independent of Re and Pr. The solution of the basic-state may be obtained analytically by the use of Bessel functions with complex arguments [1]. However, in the results presented here, the equations were solved numerically using a spectral/collocation technique, which was later used as part of the instability analysis. Basic-state velocity profiles for Rayleigh numbers of 0, 100 and -100 are shown in Fig. 1. These plots show that as the magnitude of Ra increases, the buoyant forces distort the velocity profiles. When the outer wall is heated ($Ra > 0$), the flow near the wall is accelerated. In this case, to maintain a constant mass flow rate, the fluid in the center of the pipe is proportionally decelerated. When the pipe wall is cooled ($Ra < 0$), the opposite occurs. As the magnitude of Ra increases, this model will eventually predict a parallel reverse-flow region in the pipe. However, as the plot illustrates, for both $Ra > 0$ and $Ra < 0$, points of inflection appear in the basic-state velocity profiles, indicating potential for inviscid instability. This is verified by the linear-instability calculations, which demonstrate that a stable reverse flow region is impossible.

2.3. *Linear instability*

As pointed out in ref. [2], in the case of $Ra < 0$, the fluid layer is initially unstable because of the unstable

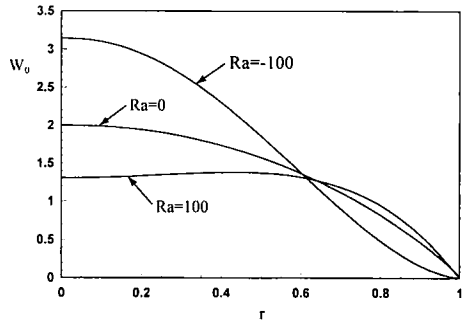

FIG. 1. Basic-state velocity profiles.

stratification. On the other hand, with $Ra > 0$, the density decreases in the vertical direction and the fluid layer is stable. Consequently, instabilities of the stably stratified case must be due to the fluid motion, while those for the unstably stratified case may be either motion-induced, or due to Rayleigh–Taylor instability. Therefore, the physical nature of the instabilities observed at $Ra > 0$ may differ substantially from those at $Ra < 0$.

The linear-instability of the basic-state is studied by subtracting the basic-state from the governing equations and neglecting the nonlinear terms. The normal mode form is assumed for the disturbances as $\psi(r, \phi, z, t) = \hat{\psi}(r)\, e^{i\alpha(z-ct)+in\phi}$, where α is the axial wave number, n the integer azimuthal wave number, $c = c_r + ic_i$ the complex disturbance wave speed and $\hat{}$ denotes a disturbance quantity. The linearized disturbance equations are

$$\hat{u}' + \frac{\hat{u}}{r} + \frac{in\hat{v}}{r} + i\alpha\hat{w} = 0 \tag{3a}$$

$$i\alpha\, Re(W-c)\hat{u} + Re\,\hat{p}' - \hat{u}'' - \frac{\hat{u}'}{r} + \frac{\hat{u}}{r^2} + \frac{n^2\hat{u}}{r^2} + \alpha^2\hat{u} + \frac{2in\hat{v}}{r^2} = 0 \tag{3b}$$

$$i\alpha\, Re(W-c)\hat{v} + \frac{in\, Re\,\hat{p}}{r} - \hat{v}'' - \frac{\hat{v}'}{r} + \frac{\hat{v}}{r^2} + \frac{n^2\hat{v}}{r^2} + \alpha^2\hat{v} - \frac{2in\hat{u}}{r^2} = 0 \tag{3c}$$

$$i\alpha\, Re(W-c)\hat{w} + Re\,\hat{u}W' + i\alpha\, Re\,\hat{p} - \hat{w}'' - \frac{\hat{w}'}{r} + \frac{n^2\hat{w}}{r^2} + \alpha^2\hat{w} + Ra\,\hat{\theta} = 0 \tag{3d}$$

$$i\alpha\, Re\, Pr(W-c)\hat{\theta} + Re\, Pr\,\hat{u}\Theta' - \hat{\theta}'' - \frac{\hat{\theta}'}{r} + \frac{n^2\hat{\theta}}{r^2} + \alpha^2\hat{\theta} - \hat{w} = 0 \tag{3e}$$

where the $'$ denotes differentiation with respect to r. The boundary conditions at the pipe wall are:

$$\hat{u}(1) = \hat{v}(1) = \hat{w}(1) = \hat{\theta}(1) = 0.$$

As explained in ref. [1], the boundary conditions at $r = 0$ will depend on the value of the azimuthal wave number, n. For $n = 0$, they are:

$$\hat{u}(0) = \hat{v}(0) = \hat{w}'(0) = \hat{\theta}'(0) = 0.$$

For $n = 1$, they become:

$$\hat{u}(0) + i\hat{v}(0) = \hat{w}(0) = \hat{\theta}(0) = 0.$$

For $n \geqslant 2$, they are:

$$\hat{u}(0) = \hat{v}(0) = \hat{w}(0) = \hat{\theta}(0) = 0.$$

Equations (3) and the boundary conditions form an eigenvalue problem for the complex disturbance wave speed, c, with the disturbance being unstable for c_i greater than 0. As explained in ref. [1], the equations were discretized using a spectral Chebyshev collocation technique, and the stability boundary was determined by a numerical search of the (Ra, Re, Pr, α, n) space to determine that locus of points where $c_i = 0$. For particular values of Pr and Re, as the magnitude of Ra increases, the point on the neutral curve that first becomes unstable defines the minimum critical Rayleigh number, Ra_c.

2.4. *Finite-amplitude instability*

Linear-instability theory determines the point at which an infinitesimal disturbance becomes unstable, but predicts unbounded exponential growth of the disturbance. As the disturbance grows to finite size, however, nonlinear effects modify the growth rate predicted by linear theory. To study these effects, the weakly nonlinear instability theory developed in ref. [9] is applied to this problem.

To study finite-amplitude instability using weakly nonlinear theory, the dependent variables are first separated into Fourier components of a disturbance wave predicted by linear-instability theory. The equations governing the harmonic components are then solved using a perturbation expansion. In this problem, we write the Fourier expansion of, for example, the axial velocity as follows:

$$w(r, \phi, z, t) = W(r, \tau)E^0 + w_1(r, \tau)E^1 + w_2(r, \tau)E^2 + \cdots + \text{c.c} \tag{4}$$

where $E = \exp(i\alpha(z - c_r t) + in\phi)$, α and n are the wave numbers corresponding to Ra_c and c_r is the wave speed of the most unstable disturbance, given by the real portion of the eigenvalue from linear theory. In this problem, we will obtain only the lowest order correction to the exponential growth predicted by linear theory, and inclusion of E^3 and higher harmonics is not necessary.

The functions for the harmonic components are further decomposed by expanding in terms of the small parameter. Using the method of multiple scales with (t, $\tau = c_i t$) results in

$$\frac{\partial}{\partial t} = \frac{\partial}{\partial t} + c_i\frac{\partial}{\partial \tau}. \tag{5}$$

The following expansion of the E^1 wave is consistent:

$$w_1(r, \tau) = c_i^{1/2}B(\tau)w_{10}(r) + c_i^{3/2}B|B|^2 w_{11}(r) + O(c_i^{5/2}) \tag{6}$$

where B is an order-one amplitude function. The physical amplitude of the w_{10} functions is therefore $A = (c_i)^{1/2}B$. The expansion for the E^1 wave given by equation (6) leads to the following forms for the E^0 and E^2 waves:

$$W(r, \tau) = W_0(r) + c_i|B(\tau)|^2 W_1(r) + O(c_i^2) \tag{7}$$

$$w_2(r, \tau) = c_i(B(\tau))^2 w_{20}(r) + O(c_i^2). \tag{8}$$

Terms of order $(c_i)^2$ and smaller are not necessary in the present analysis. Expansions of the other dependent variables corresponding to equations (6)–(8) are

given by similar expressions. The system of harmonic equations obtained by substituting equations (5)–(8) into the governing equations may be solved sequentially in increasing powers of c_i. At order $(c_i)^0$ the only non-zero contribution is from the E^0 equations, which become those of the basic-state. Therefore, the functions W_0 and Θ_0 are given by basic-state velocity and temperature distributions, respectively. At order $(c_i)^{1/2}$, the E^1 equations become those of linear-instability, and the other harmonic components are zero. Consequently, the functions u_{10}, v_{10}, w_{10} and θ_{10} are given by the eigenvectors of linear theory at the particular values of Ra, α and n being considered. At order c_i, the equations for the E^0 and E^2 waves produce nonhomogeneous equations for the mean-flow distortion functions, W_1 and Θ_1, and for the harmonic functions, u_{20}, v_{20}, w_{20} and θ_{20}. The nonhomogeneous terms in these equations involve only the functions u_{10}, v_{10}, w_{10} and θ_{10}, which are known from lower-order analysis. Therefore, these equations may be easily solved, since the amplitude function factors out on each side of the equations and may be canceled. At order $(c_i)^{3/2}$, the E^1 equations become nonhomogeneous equations with the left-hand sides consisting of the linear-instability operators operating on the functions u_{11}, v_{11}, w_{11} and θ_{11}, and the right-hand sides consisting of terms proportional to $dB/d\tau$, B and $B|B|^2$. The coefficients of the terms on the right-hand sides consist of the functions determined from the analysis at lower orders. Since the homogeneous forms of the equations are exactly those of linear-instability theory, the integrability condition requires that the right-hand sides be orthogonal to the functions satisfying the homogeneous adjoint problem. This condition leads to a Landau equation

$$\frac{dB}{d\tau} = \alpha B + a_1 B|B|^2. \tag{9}$$

The constant a_1 is the first Landau constant, and is obtained through application of the integrability condition. Equation (9) represents a modification to the exponential growth or decay of a disturbance predicted by linear theory. If the real part of a_1 is negative, a supercritical equilibrium amplitude is predicted as $|A|^2 = c_i|B|^2 = -\alpha c_i/(a_1)_r$, where $(\ )_r$ denotes the real part. In the case of $(a_1)_r$ positive, a subcritical instability is predicted with a threshold amplitude of $|A|^2 = |\alpha c_i/(a_1)_r|$.

In addition to the disturbance amplitude, the weakly nonlinear theory predicts the following order c_i modulation to the wave speed due to the disturbance growth [10]

$$c_r' = c_r + c_i \frac{(a_1)_i}{(a_1)_r} \tag{10}$$

where c_r is the wave speed predicted by linear theory, and $(a_1)_i$ is the imaginary portion of the first Landau constant.

3. RESULTS AND DISCUSSION

3.1. *Review of linear-instability results*

Figure 2 is a diagram of the linear-instability boundary for water ($Pr = 6$) in the Ra–Re plane. Positive values of Ra imply stably stratified flow, and negative Ra means the flow is unstably stratified. As mentioned in refs. [1, 2] the least stable azimuthal mode is always $n = 1$ for unstably stratified flow, and is also $n = 1$ for the stably stratified case except for a small range of Re between 50 and 150, where $n = 0$ is less stable. In both cases, the least stable Ra is almost independent of Re for $Re > 50$. Since the experimental results for water [5, 6] are at $Re > 50$, in this paper we concentrate on the results at a single value of Re equal to 600, since all the important features of the results for other Re in this range are found to be identical. Furthermore, at small Re, the results are unreliable since the mean flow has been scaled by the average velocity, which is approaching zero in this region. In this limit, the problem has a unique stability character which may be investigated by defining a dimensionless temperature based on the rate of mean temperature increase in the fluid [11].

Since it is known that isothermal flow in a circular pipe is unconditionally stable to infinitesimal disturbances [12], the linear-instabilities shown on Fig. 2 must be either of the thermal-shear, thermal-buoyant or Rayleigh–Taylor type. This may be determined by investigation of the production and dissipation of disturbance kinetic energy at the neutral curve. The balance of disturbance kinetic energy for an infinitesimal disturbance is given by

$$\frac{\partial}{\partial t}\langle \hat{u}^2 + \hat{v}^2 + \hat{w}^2 \rangle = -\left\langle \hat{u}\hat{w}\frac{dW}{dr} \right\rangle - \frac{Ra}{Re}\langle \hat{w}\hat{\theta} \rangle$$

$$-\frac{1}{Re}\langle (\nabla\hat{u})^2 + (\nabla\hat{v})^2 + (\nabla\hat{w})^2 \rangle = E_s + E_b + E_d \tag{11}$$

where the brackets $\langle\ \rangle$ imply integration over the volume of the disturbance wave. The integrals in equation (11) may be evaluated by making use of the eigenvectors obtained in the linear-instability analysis. As equation (11) demonstrates, at the neutral curve a steady balance between the production and dissipation of disturbance energy is maintained. The first

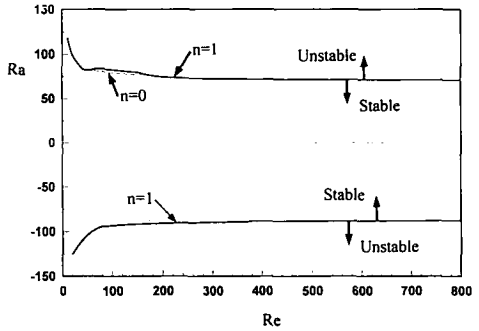

FIG. 2. Linear-instability boundary in Ra–Re plane.

term in equation (11) represents the shear production of energy due to the Reynolds stress/mean-flow strain-rate interaction. The second term represents the production of kinetic energy from the buoyant potential due to the fluctuating body force, and the last term represents the dissipation of kinetic energy due to viscous action. As this equation shows, in non-isothermal flow, the disturbance kinetic energy may be obtained from two sources in a thermally induced instability. If the shear production is dominant, the instability will be of the thermal-shear type, while if the buoyant production is pre-eminent, the instability will be either a thermal-buoyant or a Rayleigh–Taylor mode.

In this case, at $Re = 600$, in stably stratified flow, the results demonstrate that $E_b = 1.09$, $E_s = -0.09$ and $E_d = -1.0$. Therefore, this is the thermal-buoyant mode, since the Rayleigh–Taylor mode does not appear with $Ra > 0$. This is the expected result, since it has been demonstrated in ref. [8] that, in a heated annulus, the thermal-buoyant mode will be dominant for $Pr > 2.5$. In the case of unstable stratification at this Re, the buoyant mechanism is also dominant, $E_b = 1.01$, $E_s = -0.01$ and $E_d = -1.0$. In this case, however, it is not clear whether the instability is the thermal-buoyant or the Rayleigh–Taylor mode, since they both obtain most of their energy from the buoyant mechanism. However, we find that the least stable thermal instability is the Rayleigh–Taylor mode, since the disturbance appears as two long traveling waves moving in opposite directions, one on each side of the pipe [8].

3.2. *Nonlinear results*

Figure 3 is a plot of the linear-instability boundary in (Ra–α) space at $Re = 600$, $Pr = 6$ and $n = 1$ for stably stratified flow. As this plot illustrates, the critical value of Ra does not vary a great deal for a wide band of axial wave numbers. For example, the least stable point on this curve is $Ra_c = 70$ at $\alpha = 0.1$. However, by $Ra = 75$, the flow is linearly unstable for all wave numbers between $\alpha = 0.04$ and 2.7. Therefore, as Ra increases, the mode that will be amplified is not clear from this analysis, since any of the potentially unstable waves may grow and interact with other unstable modes. Because of the wide band nature of this instability, prediction of the detailed flow patterns and temperature distributions at points away from the neutral curve is beyond the scope of the classical weakly nonlinear theory. On the other hand, the results are still formally valid in the limit as Ra approaches Ra_c, and, consequently, the analysis may be used to explain the initial trends in the transition process.

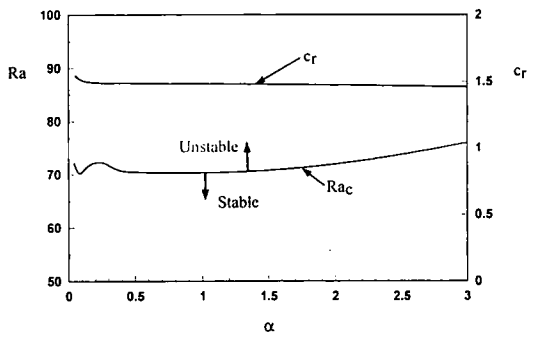

FIG. 3. Linear-instability boundary in Ra–α plane and c_r vs α at $Re = 600$ for $Ra > 0$.

The values of a_1 at selected points along the neutral curve shown in Fig. 3 are given in Table 1. The results in Table 1 show that a_{1r} is negative for all wave numbers. Therefore, this analysis predicts supercritical instability, in agreement with the experimental observations. The results in Table 1 also show that the magnitude of a_{1r} increases with increasing α at this condition. As mentioned in Section 2.4, the physical amplitude of supercritical disturbances is given by $|A|^2 = -\alpha c_i a_{1r}$, with the numerical value of a_{1r} depending on the normalization chosen for the eigenvectors obtained from linear-instability theory. Therefore, for constant values of c_i and a_{1r}, the shorter wavelength (larger wave number) disturbance will amplify faster. The results in Table 1 indicate, however, that the rate of increase of the magnitude of a_{1r} with increasing wave number more than compensates for this effect, and that the long wavelength disturbances will be amplified faster. On the other hand, the kinematics of long wavelength disturbances associated with small wave numbers result in minimal amounts of transverse mixing of the fluid. Consequently, their effects on heat transfer and friction coefficients are proportionally smaller than those of similar waves of shorter wave lengths, where the transverse velocity components will be larger.

As may be concluded from equation (10), for supercritical instability if the value of a_{1i} is negative, the growth of the disturbance will increase the wave speed, while the opposite will occur for positive a_{1i}. Therefore, the results in Table 1 show that the wave speed of the long wavelength disturbances, with $\alpha < 0.2$, will be slowed slightly by the disturbance growth. On the other hand, with $\alpha > 0.2$, the disturbances will be accelerated, and the observed wave speeds will be

Table 1. Values of the first Landau constant at the neutral curve for $Ra > 0$

Re	Ra_c	α	a_1
600	71.4	0.05	−1.20+0.70i
600	70.0	0.075	−2.60+1.30i
600	70.9	0.1	−4.49+1.55i
600	72.7	0.2	−14.6+0.10i
600	70.8	0.4	−54.4−15.1i
600	70.4	0.6	−115−54.4i
600	70.4	1.0	−273−210i
600	71.3	1.5	−483−507i
600	72.6	2.0	−652−964i
600	74.3	2.5	−745−1441i
600	76.4	3.0	−761−1907i

higher than those predicted by linear-instability theory.

It is worthwhile to mention that the weakly nonlinear theory will fail if the complex wave speed of the fundamental wave is an eigenvalue of the homogeneous form of the harmonic equations. Intuitively, this seems an unlikely contingency. However, in this problem we do find that the eigenvalue is insensitive to changes in wave number for stably stratified flow. To illustrate this, consider the plot of c_r vs the axial wave number in Fig. 3, for stably stratified flow at $Re = 600$. These results show that the wave speed c_r does not vary significantly with α. The neutral curve, also shown in Fig. 3, represents the point $c_i = 0$, and as has been discussed, Ra_c is likewise insensitive to changes in α. Since the eigenvalues of the fundamental and harmonic problems are never found to be identical, there is no theoretical difficulty in solving the equations. However, the numerical values of the eigenvalues are close enough so that care must be taken to avoid numerical difficulties in the computation of the harmonic functions. In addition, these results imply that linearly unstable oscillations of the harmonic wave may not be ignored except very near the neutral curve.

The linear-instability boundary in the (Ra–α) space at $Re = 600$ for unstably stratified flow at $Re = 600$ is shown in Fig. 4. As mentioned earlier, in this case the least stable thermal mode is the Rayleigh–Taylor instability which is a long-wavelength instability as the figure illustrates. However, a dip in the neutral curve near $\alpha = 0.8$ is caused by the presence of the asymmetric thermal-shear instability. Comparison of this result with Fig. 3 illustrates the instability boundary for this case encompasses a narrower waveband than is the case with stably stratified flow.

The results of the calculation of a_{1r} for $Ra < 0$ at $Re = 600$ are given in Table 2. Since a_{1r} is positive at $\alpha = 0.10$, these results indicate that the flow is potentially subcritically unstable, in agreement with the experimental observations. On the other hand, the value of a_{1r} is negative over most of the neutral curve. This is illustrated in Fig. 4, where the neutral curve is represented by a broken line when $a_{1r} > 0$, while a solid line indicates $a_{1r} < 0$. As these results show, only

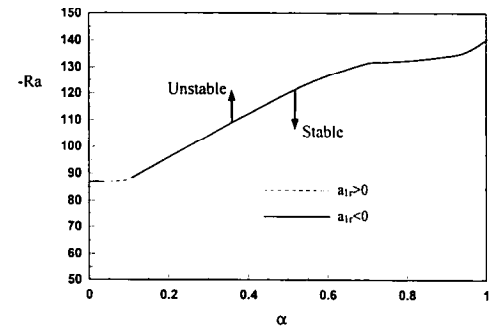

FIG. 4. Linear-instability boundary in Ra–α plane at $Re = 600$ for $Ra < 0$.

Table 2. Values of the first Landau constant at the neutral curve for $Ra < 0$

Re	Ra_c	α	a_1
600	−87.2	0.05	−0.05−0.09i
600	87.3	0.10	0.07−0.2i
600	95.6	0.20	−0.20−0.52i
600	−112	0.40	−0.54−1.5li
600	−127	0.60	−4.53−0.24i
600	−132	0.80	−65.7+4.92i
600	−136	1.0	−107+0.40i

a relatively narrow band of wave numbers, from $\alpha = 0.07$ to 0.13, are found to be subcritically unstable. In addition, the magnitude of the Landau constant in this region is relatively small, indicating that a large amplitude disturbance will be necessary to initiate subcritical instability. On the other hand, the value of a_{1r} is also small at supercritical wave numbers, which indicates that the amplitude of a supercritical disturbance will grow quickly as the magnitude of Ra increases. Because of the large amplitude necessary to induce subcritical instability, the results presented here indicate that a possible flow transition will first involve the rapid growth of a supercritical Rayleigh–Taylor instability with an azimuthal wave number of $n = 1$, followed by secondary instabilities that lead quickly to turbulence. This is consistent with the experimental observations of Scheele and Hanratty [5] who noted that, although the transition to turbulence was abrupt, the velocity profiles tended to become asymmetric before the unsteady motion set in.

3.3. *Discussion*

To gain further insight into the underlying physical phenomena that determine the behavior of subcritical and supercritical disturbances, the Landau equation (9) may be put in the following form [10]:

$$\frac{d|A|^2}{dt} = 2\alpha c_i|A|^2 + (P_{101} + E_{12} + P_{110} + T_{11} + D_{11})|A|^4$$

$$= \mathbf{L}_0 + \mathbf{P}_{101} + \mathbf{E}_{12} + \mathbf{P}_{110} + \mathbf{T}_{11} + \mathbf{D}_{11}. \quad (12)$$

The expressions for the terms on the right-hand side may be found in the Appendix at the end of this paper. The first term on the right-hand side of equation (12), $\mathbf{L}_0$, is the amplification rate from linear theory. $\mathbf{L}_0$ will be positive for supercritical states, and negative for subcritical states. The second term, $\mathbf{P}_{101}$, represents the decrease in the gradient production of disturbance kinetic energy due to the interaction between the fundamental disturbance and the distorted mean velocity gradient. Since the energy required for the distortion of the mean flow is obtained from the disturbance, this term will be negative, and will reduce the growth rate of a supercritical instability. The third term in equation (12), $\mathbf{E}_{12}$, accounts for the transfer of disturbance energy from the fundamental to the harmonic wave. The last three terms, $\mathbf{P}_{110}$, $\mathbf{T}_{11}$ and $\mathbf{D}_{11}$,

all arise because of distortion of the radial shape of the fundamental wave caused by the disturbance growth. Since the terms $\mathbf{P}_{101}$ and $\mathbf{E}_{12}$ lead to supercritical instability, for subcritical instability to exist, these terms must be positive and outweigh the combined effects of $\mathbf{P}_{101}$ and $\mathbf{E}_{12}$. The term $\mathbf{P}_{110}$ represents the modification of the gradient production of disturbance kinetic energy due to the change in the disturbance shape. The next term, $\mathbf{T}_{11}$, represents the modification in the buoyant production of disturbance kinetic energy due to the change in shape of the disturbance, while the last term, $\mathbf{D}_{11}$, represents a modification in the rate of viscous dissipation of kinetic energy. If $\mathbf{P}_{110}$ is positive, the disturbance contour is changing to a shape more favorable for shear production of disturbance energy. Likewise, if $\mathbf{T}_{11}$ is positive, the modified disturbance shape is more favorable for buoyant production of disturbance energy, while positive values of $\mathbf{D}_{11}$ imply a decrease in the viscous dissipation rate of the disturbance kinetic energy.

The terms in equation (12) are plotted vs the square of the disturbance amplitude for the supercritical thermal-buoyant instability at $Re = 600$, $\alpha = 0.6$ and $Ra = 70.5$ in Fig. 5. Since this flow is linearly unstable, the magnitude of $\mathbf{L}_0$ increases linearly with increasing amplitude. As these results demonstrate, $\mathrm{d}|A|^2/\mathrm{d}t$ is negative for $A > A_e$, and positive for $A < A_e$. Therefore, $A = A_e$ is a stable equilibrium point, since the disturbance amplitude will grow for $A < A_e$, and decay for $A > A_e$. The results also show that the modification in the rate of buoyant energy production, characterized by $\mathbf{T}_{11}$, increases the growth rate of the supercritical instability. However, the destabilizing effect of $\mathbf{T}_{11}$ is offset by the combined stabilizing effects of $\mathbf{P}_{110}$, $\mathbf{P}_{101}$ and $\mathbf{D}_{11}$. Of these terms, $\mathbf{P}_{110}$ is substantially smaller than $\mathbf{P}_{101}$ and $\mathbf{D}_{11}$, as the plot shows. The results also demonstrate that the transfer of energy to the harmonic, $\mathbf{E}_{12}$, is very small in this case. The conclusion is that with the supercritical thermal-buoyant mode, even though finite-amplitude effects increase the rate of buoyant production, the net rate of disturbance energy production is decreased by nonlinear effects. This is primarily due to increases in the viscous dissipation rate and the rate of transfer of energy from the fundamental wave back into the mean flow.

As has been discussed, the Rayleigh–Taylor instability has a small region of subcritical instability between $\alpha = 0.07$ and 0.13. To investigate the processes responsible for this behavior, in Fig. 6 we plot the magnitude of the terms in equation (12) vs the ratio of the square of the disturbance amplitude and the subcritical threshold amplitude at $\alpha = 0.1$ and $Ra = 87.2$. In this case, the flow is linearly stable, and $\mathbf{L}_0$ decreases linearly with increasing amplitude. The results also show that the point $A = A_1$ is an unstable equilibrium point since the disturbance will grow if $A > A_1$, and decay if $A < A_1$. As with the supercritical thermal-buoyant mode, in this case, the disturbance growth rate is decreased by $\mathbf{E}_{12}$ and $\mathbf{P}_{101}$. In addition, the transfer of energy from the fundamental wave to the harmonic, characterized by $\mathbf{E}_{12}$, is much more significant for this instability, while the transfer of energy from the disturbance back into the mean flow is of less importance, as Fig. 6 illustrates. In this case, however, the stabilizing effects of these terms are overcome by the combined destabilizing effects of the terms arising from the change in the shape of the fundamental wave, $\mathbf{P}_{110}$, $\mathbf{T}_{11}$ and $\mathbf{D}_{11}$. As with the thermal-buoyant instability, the increase in the rate of buoyant production of energy is the largest destabilizing term. However, the decrease in viscous dissipation and the increase in gradient production are also significant, as Fig. 6 illustrates. Therefore, in this case, subcritical instability will occur as the disturbance amplitude increases when the combined destabilizing effects caused by the change in the shape of the fundamental wave become larger than the stabilizing effects due to the production of the harmonic wave and the distortion of the mean-flow.

As has been pointed out, in this problem the range of accuracy of the weakly nonlinear expansion is limited to the region very near the neutral curve because of the large wave band of disturbances that become unstable at nearly the same value of Ra, in particular for the case of stably stratified flow. This is because the assumption of a single dominant mode is strictly justifiable only in this limit. This limitation occurs

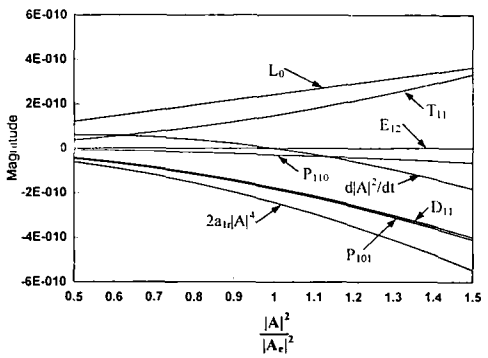

FIG. 5. Plot of terms in equation (12) vs amplitude ratio for supercritical thermal-buoyant instability with $Ra > 0$.

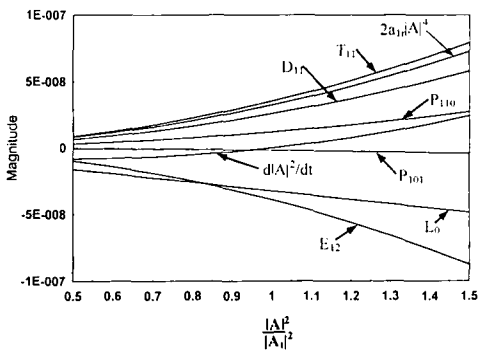

FIG. 6. Plot of terms in equation (12) vs amplitude ratio for subcritical Rayleigh–Taylor instability with $Ra < 0$.

because the weakly nonlinear theory ignores linearly unstable modes of the harmonic wave and assumes it is forced entirely by the fundamental. The presumption will be valid if the fundamental wave is amplified ($c_{i1} > 0$) while all eigenmodes of the harmonic wave are damped ($c_{i2} < 0$). Furthermore, even if the harmonic wave is itself linearly unstable, ($c_{i2} > 0$), the forced components will dominate if $|c_{i1}| \gg |c_{i2}|$. However, if $c_{i2} \sim c_{i1}$, unstable eigenmodes of the harmonic wave will appear which are the same order as those of the fundamental wave, and the waves will interact at second order. To study these phenomena requires development of a wave-interaction theory for a continuous spectrum of unstable waves, which we are presently undertaking.

3.4. *Effects on heat transfer*

A Nusselt number may be defined for this problem as

$$Nu = \frac{hr_0}{k} = \frac{\frac{1}{2}\frac{\partial\Theta(1)}{\partial r}}{\int_0^1 W\Theta r\,\mathrm{d}r} \tag{13}$$

where h is the convective heat transfer coefficient and k the fluid thermal conductivity. The Nusselt number may be determined by substituting the results of the weakly nonlinear calculations into equation (7), and evaluating the terms in equation (13). The results of this calculation for $Re = 600$ and $Ra > 0$ at a wave number of $\alpha = 1$ are given by the single-wave results in Fig. 7. In this case, supercritical flow instability occurs at $Ra = 70.5$, and the change in the rate of increase of Nusselt number with increasing Ra is evident at this point. This demonstrates that heat transfer correlations obtained analytically by use of the parallel flow assumption are inadequate in mixed-convection. For Ra slightly larger than $Ra_c = 70.4$, the increase in the heat transfer rate predicted by this model will be accurate, since the analysis is valid in the limit as $Ra \to Ra_c$. On the other hand, although precise numerical results were not presented at values of Ra that were this small, the plot of Nusselt number vs Ra from the experimental work of ref. [3] indicates that the increase in Nu due to instability is about 20% at $Ra = 100$, while the single-wave weakly nonlinear theory predicts a much smaller increase in Nusselt number due to instability at this point, as Fig. 7 illustrates. This is not surprising, since, as discussed in the previous section, in this flow a continuous band of waves become unstable at nearly the same time. Unfortunately, no detailed experimental measurements of the unsteady flow patterns are available to indicate which of the unstable waves become dominant. However, the effect of multiple waves may be accounted for approximately by ignoring wave interactions and including the contributions from each wave individually. If this approach is taken, the Nusselt number may be written as follows:

$$Nu = Nu_0 + \sum_{i=1}^{N} Nu_i \tag{14}$$

where Nu_0 is the Nusselt number due to the basic-state, and the Nu_i are the individual contributions of each of the N unstable waves. Figure 7 also includes plots of Nu vs Ra at $Re = 600$ for four and eight waves. As these results show, a more substantial increase in heat transfer is obtained by this model, with the eight wave model predicting the experimentally observed increase in Nu of 20% at $Ra = 100$. However, since the results depend on the number of waves present, unless detailed experimental measurements become available which would allow a proper choice of wave numbers to be included in the model, it is difficult to make conclusions about the detailed structure of the unsteady flow. In addition, this analysis does not include the nonlinear interactions which will be present among the unstable waves.

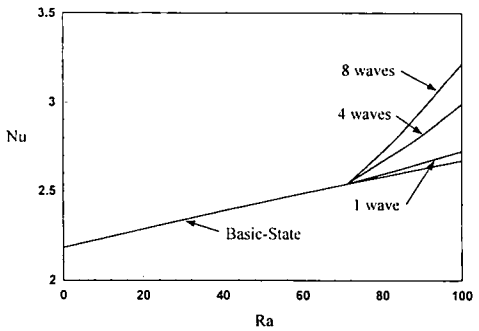

FIG. 7. Nu vs Ra at $Re = 600$.

4. CONCLUSIONS

Analysis of the energy transfer for the instability of stably stratified flow in a heated vertical pipe has shown that this is the thermal-buoyant instability. The weakly nonlinear instability theory has predicted supercritical instability for all wave numbers, in agreement with the experimental observations. Analysis of the terms which make up the real part of the Landau constant shows this instability is supercritical because increases in the viscous dissipation rate and the rate of transfer of energy from the fundamental wave back into the mean flow overcome the destabilizing effect of an increase in the rate of buoyant production. It is found that a wide band of wave numbers become linearly unstable soon after the initial instability. Therefore, even though the weakly nonlinear theory is valid in the limit as Ra approaches Ra_c, the theory will be inaccurate as Ra increases, since it considers only a single dominant wave. As expected the increase in Nusselt number due to flow instability predicted by the single-wave theory is smaller than the experimentally observed values. This is due to the fact that the instability involves more than the most unstable wave. A complete description of the phenomena

requires consideration of a continuous band of unstable waves, which is currently being studied.

The results for the unstably stratified case demonstrate that this instability is the Rayleigh–Taylor mode. The weakly nonlinear calculations indicate that the flow is potentially subcritically unstable, again in agreement with the experimental observations. The subcritical instability occurs when the disturbance amplitude increases to the point that the combined destabilizing effects caused by the change in the shape of the fundamental wave become larger than the stabilizing effects due to the production of the harmonic wave and the distortion of the mean-flow. On the other hand, the weakly nonlinear theory predicts that a large amplitude disturbance will be necessary to initiate subcritical instability, while the amplitude of a supercritical disturbance will grow quickly as the magnitude of Ra increases. Therefore, a possible flow transition will first involve the rapid growth of a supercritical Rayleigh–Taylor instability with an azimuthal wave number of $n = 1$, followed by secondary instabilities that lead quickly to turbulence. This is consistent with the experimental observations of Scheele and Hanratty [5] who noted that, although the transition to turbulence was abrupt, the velocity profiles tended to become asymmetric before the unsteady motion set in.

Acknowledgement—Funding for this work is provided by the National Science Foundation under Grants CTS 89-13537.

REFERENCES

1. L. S. Yao, Is fully developed and non-isothermal flow possible in a vertical pipe? *Int. J. Heat Mass Transfer* **30**, 707–716 (1987).
2. L. S. Yao, Linear stability analysis for opposing mixed convection in a vertial pipe, *Int. J. Heat Mass Transfer* **30**, 810–811 (1987).
3. T. J. Hanratty, E. M. Rosen and R. L. Kabel, Effect of heat transfer on flow field at low Reynolds numbers in vertical tubes, *Ind. Engng Chem.* **50**, 815–820 (1958).
4. G. A. Kemeny and E. V. Somers, Combined free and forced convection in vertical circular tubes—experiments with water and oil, *Trans. ASME C. J. Heat Transfer* **108**, 392–397 (1962).
5. G. F. Scheele and T. J. Hanratty, Effect of natural convection on stability of flow in a vertical pipe, *J. Fluid Mech.* **14**, 244–256 (1962).
6. L. S. Yao and B. B. Rogers, The linear stability of mixed convection in a vertical annulus, *J. Fluid Mech.* **201**, 279–298 (1989).
7. L. S. Yao and B. B. Rogers, Mixed convection in an annulus of large aspect ratio, *J. Heat Transfer* **111**, 683–689 (1989).
8. B. B. Rogers and L. S. Yao, The importance of Prandtl number in mixed-convection instability, *J. Heat Transfer* (in press).
9. L. S. Yao and B. B. Rogers, Finite-amplitude instability of nonisothermal flow in a vertical annulus, *Proc. R. Soc. Lond. A* **437**, 267–290 (1992).
10. J. T. Stuart, On the non-linear mechanics of wave disturbances in stable and unstable parallel flows, *J. Fluid Mech.* **54**, 93–112 (1960).
11. B. B. Rogers and L. S. Yao, Natural convection in a heated annulus, *Int. J. Heat Mass Transfer* **36**, 35–47 (1993).
12. A. Davey and H. P. F. Nguyen, Finite-amplitude stability of pipe flow, *J. Fluid Mech.* **45**, 701–720 (1971).

APPENDIX

The balance of kinetic energy contained in the fundamental wave results in the following equation:

$$\frac{\partial}{\partial t}\langle \tfrac{1}{2}[\overline{u_1^2}+\overline{v_1^2}+\overline{w_1^2}]\rangle = -\left\langle \overline{u_1 w_1}\frac{\partial W}{\partial r}\right\rangle - \frac{Ra}{Re}\langle \overline{w_1\theta_1}\rangle$$
$$-\frac{1}{Re}\left\langle \overline{\left(\frac{\partial u_1}{\partial r}\right)^2}+\overline{\left(\frac{1}{r}\frac{\partial u_1}{\partial \phi}\right)^2}+\overline{\left(\frac{\partial u_1}{\partial z}\right)^2}+\overline{\left(\frac{\partial v_1}{\partial r}\right)^2}\right.$$
$$\left.+\overline{\left(\frac{1}{r}\frac{\partial v_1}{\partial \phi}\right)^2}+\overline{\left(\frac{\partial v_1}{\partial z}\right)^2}+\overline{\left(\frac{1}{r}\frac{\partial v_1}{\partial \phi}\right)^2}+\overline{\left(\frac{\partial w_1}{\partial r}\right)^2}+\overline{\left(\frac{\partial w_1}{\partial z}\right)^2}\right\rangle$$
$$-\left\langle \overline{u_1^2}\frac{\partial u_2}{\partial r}+\frac{\overline{u_1 v_1}}{r}\frac{\partial u_2}{\partial \phi}+\overline{u_1 w_1}\frac{\partial u_2}{\partial z}+\overline{u_1 v_1}\frac{\partial v_2}{\partial r}\right.$$
$$\left.+\frac{\overline{v_1^2}}{r}\frac{\partial v_2}{\partial \phi}+\overline{w_1 v_1}\frac{\partial v_2}{\partial z}+\overline{u_1 w_1}\frac{\partial w_2}{\partial r}+\frac{\overline{w_1 v_1}}{r}\frac{\partial w_2}{\partial \phi}+\overline{w_1^2}\frac{\partial w_2}{\partial z}\right\rangle \tag{A1}$$

where the overbar implies the spatial mean and the brackets $\langle\ \rangle$ imply integration over the volume of the wave. As equation (12) implies, if equations (6)–(8) are substituted into equation (A1), the equation which results will be of the same form as the real part of equation (9). The formulas for the terms in equation (12) are given below.

$$e_0 = \tfrac{1}{2}\langle \overline{u_{10}^2}+\overline{v_{10}^2}+\overline{w_{10}^2}\rangle \tag{A2}$$

$$\mathbf{P}_{101} = -\frac{1}{e_0}\left\langle \overline{u_{10}w_{10}}\frac{dW_1}{dr}\right\rangle \tag{A3}$$

$$E_{12} = -\frac{1}{e_0}\left\langle \overline{u_{10}^2}\overline{\frac{\partial u_{20}}{\partial r}}+\overline{\frac{u_{10}v_{10}}{r}\frac{\partial u_{20}}{\partial \phi}}+\overline{u_{10}w_{10}\frac{\partial u_{20}}{\partial z}}\right.$$
$$+\overline{u_{10}v_{10}}\overline{\frac{\partial v_{20}}{\partial r}}+\overline{\frac{v_{10}^2}{r}\frac{\partial v_{20}}{\partial \phi}}+\overline{v_{10}w_{10}\frac{\partial v_{20}}{\partial z}}$$
$$\left.+\overline{u_{10}v_{10}}\overline{\frac{\partial w_{20}}{\partial r}}+\overline{\frac{w_{10}v_{10}}{r}\frac{\partial w_{20}}{\partial \phi}}+\overline{w_{10}^2\frac{\partial u_{20}}{\partial z}}\right\rangle \tag{A4}$$

$$\mathbf{P}_{110} = -\frac{1}{e_0}\left\langle (\overline{u_{10}w_{11}}+\overline{u_{11}w_{10}})\frac{dW_0}{dr}\right\rangle \tag{A5}$$

$$T_{11} = -\frac{Ra}{e_0 Re}\langle (\overline{\theta_{10}w_{11}}+\overline{\theta_{11}w_{10}})\rangle \tag{A6}$$

$$D_{11} = -\frac{1}{e_0 Re}\left\langle \overline{\frac{\partial u_{10}}{\partial r}\frac{\partial u_{11}}{\partial r}}+\overline{\frac{1}{r}\frac{\partial u_{10}}{\partial \phi}\frac{\partial u_{11}}{\partial \phi}}+\overline{\frac{\partial u_{10}}{\partial z}\frac{\partial u_{11}}{\partial z}}\right.$$
$$+\overline{\frac{\partial v_{10}}{\partial r}\frac{\partial v_{11}}{\partial r}}+\overline{\frac{1}{r}\frac{\partial v_{10}}{\partial \phi}\frac{\partial v_{11}}{\partial \phi}}+\overline{\frac{\partial v_{10}}{\partial z}\frac{\partial v_{11}}{\partial z}}$$
$$\left.+\overline{\frac{\partial w_{10}}{\partial r}\frac{\partial w_{11}}{\partial r}}+\overline{\frac{1}{r}\frac{\partial w_{10}}{\partial \phi}\frac{\partial w_{11}}{\partial \phi}}+\overline{\frac{\partial w_{10}}{\partial z}\frac{\partial w_{11}}{\partial z}}\right\rangle. \tag{A7}$$